applied sciences

MDPI

Article

Direct Measurements of Cosmic Rays (TeV and beyond) Using an Ultrathin Calorimeter: Lessening Fluctuation Method

Igor Lebedev [1,*], Anastasia Fedosimova [2,*], Andrey Mayorov [3], Pavel Krassovitskiy [4], Elena Dmitriyeva [1], Sayora Ibraimova [1] and Ekaterina Bondar [1]

[1] Institute of Physics and Technology, Satbayev University, Almaty 050032, Kazakhstan; dmitriyeva2017@mail.ru (E.D.); sayara_ibraimova@mail.ru (S.I.); grushevskaiya@bk.ru (E.B.)
[2] Faculty of Physics and Technology, Al-Farabi Kazakh National University, Almaty 050040, Kazakhstan
[3] Department of Experimental Nuclear and Space Physics, Moscow Engineering and Physics Institute, National Research Nuclear University MEPhI, 115409 Moscow, Russia; agmayorov@mephi.ru
[4] Laboratory of Theoretical Nuclear Physics, Institute of Nuclear Physics, Almaty 050032, Kazakhstan; pavel.kras@inp.kz
* Correspondence: lebedev692007@yandex.ru (I.L.); ananastasia@list.ru (A.F.)

Abstract: In this paper, we propose a method that makes it possible to use an ultrathin calorimeter for direct measurements of cosmic rays with energies of TeV and higher. The problems of determining the primary energy with a thin calorimeter, due to large fluctuations in shower development, the low statistics of analyzed events and the large size required for the calorimeter, are considered in detail. A solution to these problems is proposed on the basis of a lessening fluctuation method. This method is based on the assumption of the universality of the development of cascades initiated by particles of the same energy and mass. For energy reconstruction, so-called correlation curves are used. The main analyzed quantities are the size of the cascade and the rate of its development. The method was tested using the calorimeter of the PAMELA collaboration. Based on simulations, it is shown that the primary energy can be determined on the ascending branch of the cascade curve. This fact solves the problems associated with the need to increase the calorimeter thickness with an increase in primary energy and with the limitation of the analyzed events. The proposed technique is universal for different energies and different nuclei.

Keywords: ultrathin calorimeter; cosmic rays; direct measurements; energy reconstruction; PAMELA; shower development universality

Citation: Lebedev, I.; Fedosimova, A.; Mayorov, A.; Krassovitskiy, P.; Dmitriyeva, E.; Ibraimova, S.; Bondar, E. Direct Measurements of Cosmic Rays (TeV and beyond) Using an Ultrathin Calorimeter: Lessening Fluctuation Method. *Appl. Sci.* **2021**, *11*, 11189. https://doi.org/10.3390/app112311189

Academic Editors: Roberta Sparvoli and Matteo Martucci

Received: 9 October 2021
Accepted: 22 November 2021
Published: 25 November 2021

1. Introduction

Measurements of the chemical composition and fluxes of cosmic rays play a decisive role in understanding the mechanisms of their acceleration and propagation. Different cosmological models predict different elemental composition of cosmic rays and different spectra of the elements [1–3].

Cosmic rays at energies E > 100 TeV are studied at ground-based cosmic ray stations based on the analysis of extensive air showers [4,5]. Cosmic rays at E < 100 TeV are studied by direct measurements outside the Earth's atmosphere on spacecraft or high-altitude aerostats. The main advantage of direct experiments is the ability to measure the charge of the incident particle.

The energies of cosmic particles are measured fairly accurately for particles with energies E < 100 GeV. Modern magnetic spectrometers can detect the primary energy with an error of less than 10 percent. Such devices have limitations at energies of TeV and higher [6–8].

In the region of 1–100 TeV, there is a lack of experimental methods. Today, there is practically only one reliable method for measuring the energy of various nuclei at energies of TeV and above: this is the ionization calorimeter method [9,10].

At present, calorimeters are used in almost all experiments in the study of cosmic rays, in which the equipment is placed on high-altitude balloons or spacecraft. The main problem with this method of measuring energy is that it requires heavy devices, since the calorimeter must have sufficient depth to determine the value of the total energy release in the calorimeter. Moreover, the higher the primary energy, the thicker the calorimeter should be. The huge weight of the installation makes it much more difficult to use such a device in space experiments.

A more promising approach to determining the energy of cosmic rays based on direct measurements is the use of a thin calorimeter. In a thin calorimeter, the entire cascade of secondary particles is not recorded, but only the beginning of the cascade is measured. Many methods have been developed for measuring the energy of the initial particles using various types of thin calorimeters. However, due to significant fluctuations in the development of the cascade, the energy resolution of thin calorimeters when measuring hadron cascades at the present stage is 30–70% [11–19].

Most of the energy measurement methods used in modern experiments are based on the use of a cascade curve—the dependence of the cascade size (usually, the logarithm of the energy release, $\log q$, at the calorimeter measurement layer is used) on the penetration depth (d) of cascade to this measurement layer.

If the cascade curve has reached its maximum in the calorimeter, then the primary energy is reconstructed quite accurately. However, in order to measure the maximum of the cascade, the calorimeter must have a sufficiently large thickness. Moreover, the higher the primary energy, the thicker the calorimeter should be.

If the maximum of the cascade curve is not reached in the calorimeter, then the energy release at the last layer of the calorimeter, or the total energy release in the calorimeter, is used to determine the energy. Cascade curves fluctuate significantly. The cascade can begin to develop on the first measurement layer, for example, or on the 10th measurement layer. Accordingly, the total energy release in the calorimeter for these two cascades will differ significantly. Furthermore, since total energy release is used to define primary energy, large fluctuations in total energy release lead to large errors in primary energy reconstruction.

This paper presents a lessening fluctuation method (LFM) to improve energy reconstruction for data obtained with thin calorimeters. The proposed method is based on the use of so-called correlation curves—the dependence of the cascade size ($S = \log q$) on the cascade development rate (R). The cascade development rate is understood as a value equal to the difference in the cascade size at two measurement levels, divided by the calorimeter thickness, during the passage of which this change in the cascade size occurs: $R = (S_1 - S_2)/(d_1 - d_2)$, where d_1 and d_2 are the penetration depths to these two measurement layers. The cascade development rate depends on the primary energy and, therefore, can be used as an additional value to improve the accuracy of the reconstruction of the primary energy. The size–rate curves practically do not fluctuate. They coincide with the cascade, which begins to develop at the first measuring layer, and the cascade, which begins at the 10th measuring layer. Therefore, the energy resolution is better than using cascade curves.

Moreover, using this method, the primary energy is reconstructed near the beginning of the development of the cascade. Thus, with increasing energy, it is not necessary to increase the calorimeter thickness. Moreover, the calorimeter thickness can be reduced and an ultrathin calorimeter used.

2. Primary Energy Measurement with a Calorimeter

The technical realization of modern ionization calorimeters can be variable, but the idea remains invariable: the primary particle enters into a dense substance (absorber), in which numerous nuclear and electromagnetic interactions take place. It gives rise to a cascade of secondary particles. To measure the characteristics of the cascade, the dense substance is sandwiched with special detectors. By measurement of signals from these detectors, the cascade curve is formed.

By their design, calorimeters are divided into homogeneous and heterogeneous. Heterogeneous calorimeters consist of layers of a substance with a high density (lead, tungsten), where particles lose their energy during passage, alternating with layers of detectors (silicon), where the energy released by the particles of the cascade is measured. Homogeneous calorimeters use substances (bismuth germanate crystal, lead tungstate, etc.) which are simultaneously both an absorber and a detector.

The geometric dimensions of heterogeneous calorimeters are usually significantly lower than those of homogeneous ones. In addition, they have better spatial resolution as they are segmented in both the longitudinal and lateral directions. A significant drawback of heterogeneous calorimeters is the transient effect due to the significant difference in the densities of the absorber and detector. Cascade curves develop differently in different materials. Consequently, the behavior of the cascade curve is violated when the cascade transitions from one material to another. In this regard, fluctuations in the development of the cascade from layer to layer can be observed. The strongest fluctuations from layer to layer are at the beginning of the development of the cascade. This makes the analysis very difficult [20].

Several methods have been developed to measure the primary energy of cosmic rays using different types of calorimeters.

The PAMELA calorimeter is a heterogeneous calorimeter. It consists of 22(x, y) silicon detector planes alternating with tungsten absorber planes. The calorimeter thickness is 16.3 radiation lengths. In the PAMELA experiment, the primary energy is estimated from the maximum of the cascade curve describing the longitudinal profile of the shower developed in the calorimeter. If the shower maximum is located outside the calorimeter, then the energy released in the last layer of the calorimeter is used to estimate the energy. This technique provides an energy resolution for protons of ~40% [14].

The NUCLEON calorimeter thickness is 15.3 radiation lengths (the silicon microstrip detectors interleaved with thin tungsten layers). The proposed technique for primary CR energy measurement is based on the generalized Castagnoli kinematical method (KLEM method) developed for emulsion. In this method, the primary energy is reconstructed by registering the spatial density of the secondary particles. Secondary particles are generated by the first hadronic inelastic interaction in a carbon target. Additional particles are then produced in a thin tungsten converter by electro-magnetic and hadronic interactions. This method provides an energy resolution of ~70% [16].

CALET is a homogeneous calorimeter made of lead tungstate ($PbWO_4$) bars arranged in 12 layers. The total thickness of the device is equivalent to 30 radiation lengths. The primary particle energy is calculated from the total energy release in the calorimeter. The energy released in the calorimeter is scaled linearly with the energy of the incident particle. The obtained energy resolution is close to 30% [17].

ATIC is a homogeneous calorimeter consisting of 10 layers of 40 bismuth germanium scintillation crystals (BGO). The total thickness is approximately 22 radiation lengths. For protons, most of the released energy is not recorded by the calorimeter detectors. In this regard, the selection of events was carried out according to predetermined conditions, such as the interaction near the upper boundary of the calorimeter. Despite this, the energy resolution for protons is ~30% due to large fluctuations in the energy release of the hadron cascade [11].

DAMPE is a homogeneous calorimeter of about 31.5 radiation lengths. The calorimeter is made on the basis of bismuth germanate crystals. For energy reconstruction, MC simulations are used to derive the energy response matrix, applying some selections. Then a deconvolution of the measured energy distribution into the incident energy distribution is applied. The number of events in the i-th deposited energy bin is obtained via the sum of the number of events in all the incident energy bins weighted by the energy response matrix. The energy resolution for protons is approximately 35% [18].

Figure 1 shows the proton energy spectra measured in various experiments. As can be seen from Figure 1, at energies up to 100 GeV, all the presented spectra practically coincide.

At energies higher than 100 GeV, the difference becomes more significant, and the spectrum measurement errors are significantly higher.

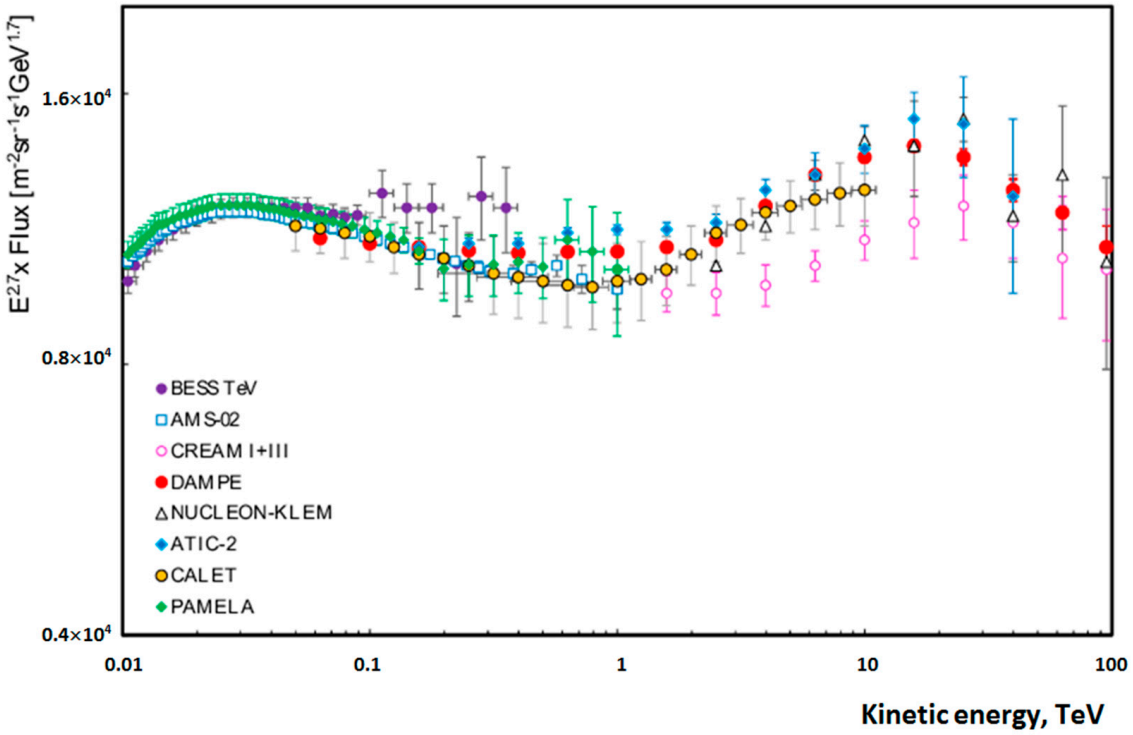

Figure 1. Proton spectra of various experiments [11–19].

Modern experiments with calorimeters for 20–30 radiation lengths do not allow measuring the entire flux of cosmic rays. Many events do not reach the maximum of the cascade and they are excluded from the analysis. Alternatively, their energy is determined with low accuracy. In this regard, the real energy spectrum is distorted. The higher the energy of the primary particle, the thicker the calorimeter should be. To lift a much larger calorimeter into space requires enormous financial cost. Therefore, it is necessary to look for ways to reduce the influence of fluctuations in the development of the cascade on the results of measuring the primary energy.

3. Lessening Fluctuation Method

LFM has been tested on the PAMELA calorimeter. Simulation of the development of cascade processes formed by primary particles of various masses and energies was carried out using the GEANT4 10.4 software package [21].

3.1. Fluctuations in Cascade Development

To determine the primary energy E based on the energy release at the observation level, usually the following dependence is used: $q = aE^b$, where a, b are parameters depending on the penetration depth d and the mass of the primary particle. The equation is statistically correct. However, q (at the observation level) strongly fluctuates in an individual event. Therefore, in order to solve the problem of large fluctuations in the development of a cascade, it is necessary to start with an analysis of fluctuations in individual events. For this, we first considered individual cascades with significantly different cascade curves.

As the analyzed value of the cascade size, we used the logarithm of the energy release, $\log q$, at the measuring layer. The measuring levels of the PAMELA calorimeter were equidistant. Therefore, as the cascade curved, we analyzed the dependence of the cascade size on the layer number, L.

The cascade, the development of which starts at the beginning of the calorimeter, is called a fast cascade. The cascade, the significant development of which begins in the second half of the calorimeter, is called a slow cascade.

Figure 2a shows the cascade curves for three cascades of 10 TeV protons with fast, medium, and slow character of the development of the cascade process.

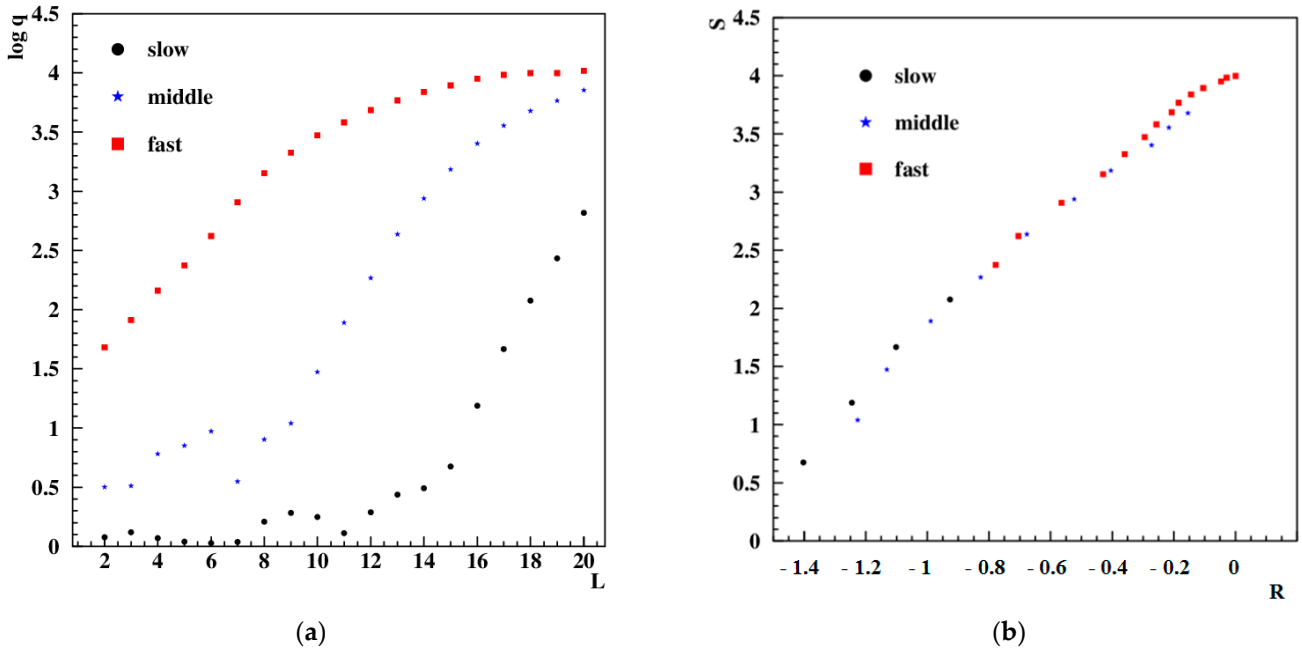

(**a**) (**b**)

Figure 2. (**a**) Cascade curves for three showers of 10 TeV protons with fast, medium, and slow character of the development of the cascade process; (**b**) The size–rate curves for the same showers.

As can be seen in Figure 2a, the total energy release in the calorimeter for these three showers differs significantly. The total energy release by the fast shower is several times higher than that released by the slow shower. Therefore, methods using this parameter to reconstruct the primary energy will determine that the energy of these showers is significantly different, while the primary energy of these showers is the same. The situation is similar for methods that use the energy release on the last calorimeter layer as a calculated value, since this value also differs significantly for these three showers.

Determination of the energy from the maximum of the cascade curve is possible only for fast showers. Slow and medium showers cannot be analyzed because they do not reach the maximum of the cascade curve. Thus, the statistics of the analyzed events are significantly reduced. Moreover, the maximum point shifts towards greater depth with increasing energy. Therefore, the higher the primary energy, the thicker the calorimeter should be.

To understand how to solve the problem of large fluctuations in the development of a cascade, it is necessary to understand what their causes are.

The behavior of the cascade curve depends on the features of the interaction of the primary nucleus with the nuclei of the calorimetric substance. Different approaches and methods are used in order to study features in the multi-particle production [22–26]. First, the fluctuations of the penetration depth before the first interaction are very important. The earlier the primary particle interacts, the faster the cascade begins to develop. Second, fluctuations in the multiplicity of the first interaction are important. If the first interaction is central, then many particles are produced and the cascade develops rapidly. If the first interaction is peripheral, then the cascade develops slowly. For example, the proton that initiated the middle cascade (Figure 2a) interacted at the beginning of the calorimeter, but the rapid development of the cascade began only after layer 9.

After the first interaction, each secondary particle can interact, also producing secondary particles. The parameters (the penetration depth before the first interaction, the number of secondary particles, etc.) of each subsequent interaction also fluctuate. However, since there are several particles in a cascade, fluctuations of individual interactions can partially compensate each other. When there are many particles in a cascade, the property of universality of the cascade development is realized. All cascades initiated by particles of the same energy and mass develop in the same way [27,28].

Thus, the cascades differ greatly in the depth of the first interaction. They also differ greatly in the parameters of the first interaction (multiplicity, peripherality, etc.). This leads to major fluctuations at the beginning of the cascade curve. However, the cascade fluctuates weakly if it contains many secondary particles. Thus, instead of the penetration depth, it is necessary to find another parameter that does not depend on these fluctuations in the development of the cascade process.

LFM is based on the use of so-called correlation curves—the dependence of the cascade size ($S = \log q$) on the cascade development rate $R = (S_1 - S_2)/(d_1 - d_2)$. As unit absorber ($d_1 - d_2$), a thickness equal to three layers of the PAMELA calorimeter was chosen. Therefore, the rate of shower development was calculated as the difference between the cascade size on the L-th and $L + 3$ measuring layers, $R = S_L - S_{L+3}$.

When choosing the thickness of the unit absorber, we took into account two main factors. The first factor was fluctuations from layer to layer. The thinner the unit absorber, the higher the relative fluctuations of R due to fluctuations from layer to layer. Therefore, it was preferable to choose a thicker unit absorber. The second factor was the calorimeter thickness. The thinner the unit absorber used in the LFM, the more points on the correlation curve could be obtained. Looking to the future, a thin unit absorber makes it possible to use an ultra-thin calorimeter to measure primary energy.

Figure 2b shows the correlation curves for the same three showers that were presented in Figure 2a. As can be seen in Figure 2b, in contrast to the cascade curves (Figure 2a), the correlation curves almost coincide for fast, medium, and slow showers.

This greatly simplifies the task of determining the primary energy. Regardless of fluctuations in the development of a shower, all proton showers of the same energy are located on the same curve. Therefore, the energy of these showers will also be defined as the same.

3.2. The Analysis Procedure: The Size–Rate Function

The analysis procedure consisted of several main stages.

First stage: simulation of cascades with fixed energies.

We simulated 100 cascades initiated by iron nuclei, 100 carbon cascades and 100 proton cascades with fixed energies of 1 TeV and 10 TeV in the PAMELA calorimeter.

The mean cascade curves for these cascades are presented in Figure 3a. Error bars show statistical errors. As can be seen in Figure 3a, the development of the proton and Fe cascades is significantly different. At $L < 8$ Fe showers with energy of 1 TeV have $\log q$ higher than proton showers with energy of 10 TeV. The most significant factors determining the observed differences are the penetration depth before the first interaction and the number of secondary particles formed.

Second stage: smoothing the cascade curve.

To reduce fluctuations from layer to layer, a signal accumulation method along the spectrum was used. This method allows for a softer minimization of fluctuations from layer to layer, in contrast, for example, to fitting with a polynomial function [29]. Smoothing was carried out at three points in accordance with the formula:

$$S_L = \frac{1}{3} \sum_{i=L-1}^{L+1} \log q_i$$

where log q_i is the measured value of the shower size, and S_L is the accumulated value of the shower size.

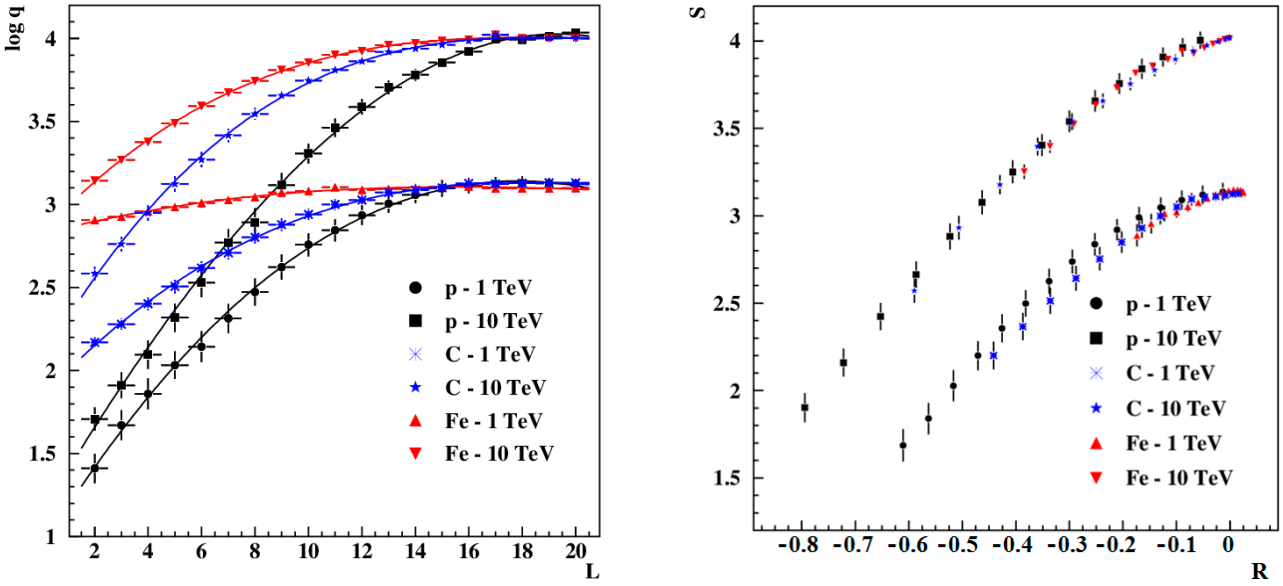

(**a**) (**b**)

Figure 3. (**a**) Cascade curves for showers initiated by protons, C and Fe nuclei with energies of 1 TeV and 10 TeV in the PAMELA calorimeter; (**b**) The size–rate curves for the same showers.

Third stage: searching for the beginning of the cascade development.

As can be seen in Figure 3a, the avalanche-like process of the cascade development does not always begin immediately after the interaction of the primary particle with the calorimeter substance. If the first interaction is peripheral, then the energy release from layer to layer can not only increase, but also decrease. We considered such cascades as not having started. In order to separate the part of the measurements in which the cascade had not yet begun, we compared the rate of development of the cascade in adjacent layers. If the rate of development of a cascade increased at three adjacent observation levels in a row, then such a cascade was considered to have begun. For example, the fast cascade shown in Figure 3a was considered to have started at the first level, the middle at layer 9, and the slow cascade only at layer 15.

Fourth stage: plotting *SR* distributions.

Figure 3b shows the average size–rate dependences for the same proton, carbon and Fe cascades as in Figure 3a.

As can be seen in Figure 3b the size–rate dependences are an ordered structure depending on the primary energy and are practically independent of the type of the primary nucleus. This fact can also be attributed to the advantages of the presented approach.

Fifth stage: creating the size–rate function.

To create the *SR* function, we fitted the *SR* curves of third-order polynomial functions for each fixed energy:

$$S\,(R) = a_0 + a_1 R + a_2 R^2 + a_3 R^3 \quad (1)$$

Then the coefficients a_0, a_1, a_2, a_3 were fitted depending on the energy. The size–rate function for reconstructing primary energy was in the following form:

$$S(R,E) = a_0(E)+a_1(E)R+a_2(E)R^2+a_3(E)R^3 \quad (2)$$

Using the size–rate function (2), an analysis of test cascades was performed.

3.3. Analysis of Test Cascades

For the analysis 100 test cascades formed by primary protons, 100 carbon cascades and 100 cascades formed by iron nuclei with random energies in the range from 1 TeV to 10 TeV were simulated.

Reconstruction of the primary energy was based on dependence (2). In order to determine the energy of the i-th test cascade using (2), it was necessary to substitute into the function (2) the "measured" value of the rate R_m and to vary E_{rec} in order to minimize the difference between "measured" value of the size S_m and the size–rate function (2):

$$| S_m - S(R_m,E_{rec}) | = | S_m - (a_0(E_{rec}) + a_1(E_{rec}) R_m + a_2(E_{rec}) {R_m}^2 + a_3(E_{rec}) {R_m}^3) | < \varepsilon$$

In the calculations, we used $\varepsilon = 0.001$. Energy reconstruction errors were calculated using the formula:

$$\sigma E = \sqrt{\frac{\sum (E - E_{rec})^2}{n-1}},$$

where n is number of reconstructed events.

Figure 4 shows the energy resolution reached by this procedure. The energy resolution is practically independent of the primary energy.

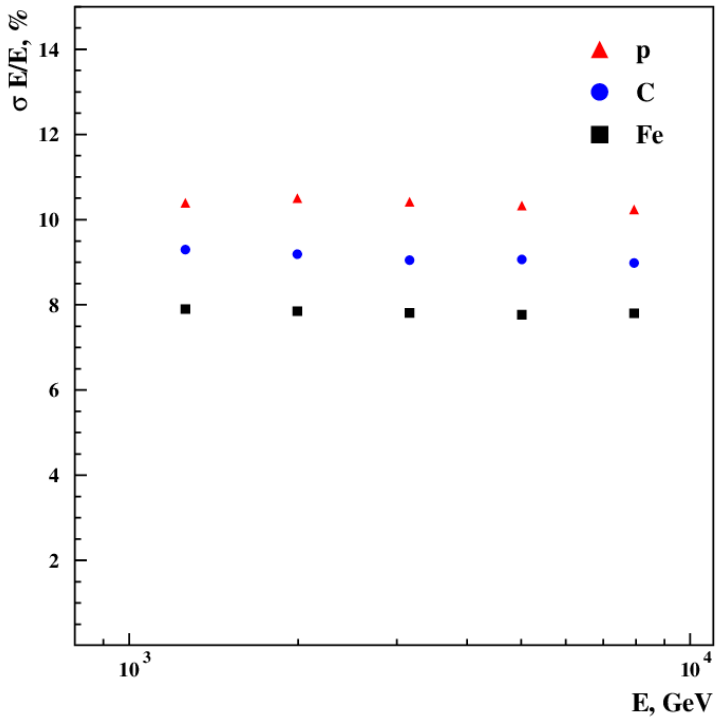

Figure 4. Energy resolution for p, C and Fe cascades at different energies in the PAMELA calorimeter.

In this paper, we did not consider the correlation between fit parameters and how they affect the ultimate energy reconstruction. It is likely that an improvement in the fitting parameters can improve the results of primary energy reconstruction.

The correlation curves presented in this paper were constructed for analysis of the PAMELA calorimeter. In case of a change in the geometry and material of the calorimeter, the analysis procedure must be repeated in full.

4. Conclusions

In this paper, we considered the possibility of using an ultrathin calorimeter for direct measurements of cosmic rays with energies TeV and higher. The following problems of measuring the energy of cosmic particles using a thin calorimeter were considered in

detail: large fluctuations in the development of cascade processes (they lead to significant errors in determining the energy); limiting the number of analyzed events (particles whose cascade curves have not reached their maximum cannot be measured and they are excluded from the analysis); large calorimeter sizes (the higher the primary energy, the thicker the calorimeter should be). A solution to these problems is proposed on the basis of a lessening fluctuation method. This method is based on the assumption of the universality of the development of cascades formed by particles of the same energy and charge. For energy reconstruction, so called, *SR* curves are used. The main analyzed quantities are: *S*—the size of the cascade (the energy deposited on each layer of the calorimeter); *R*—the rate of development of the cascade (the difference in the cascade size on two measuring layers of the calorimeter).

Based on simulations of the PAMELA calorimeter, it is shown that the *SR* curves are almost parallel to each other and practically do not depend on the depth of the cascade development. It makes it possible to determine the primary energy for cascades that have not reached their maximum. This fact solves the problem associated with the need to increase the calorimeter thickness with increasing primary energy. Therefore, an ultrathin calorimeter can be used for measurement. In addition, the statistics of the analyzed events can be increased. Correlation curves fluctuate much less than cascade curves. Therefore, the energy resolution for protons is improved by ~10 percent. The proposed technique is universal for different energies and different nuclei.

Author Contributions: Conceptualization and methodology, I.L. and A.F.; software and simulation, A.M.; analysis and investigation, E.D., S.I., P.K. and E.B. All authors have read and agreed to the published version of the manuscript.

Funding: This research was funded by the Ministry of Education and Science of the Republic of Kazakhstan grant number AP08855403.

Conflicts of Interest: The authors declare no conflict of interest.

References

1. Ptuskin, V.; Zirakashvili, V.; Seo, E.S. Spectra of cosmic-ray protons and helium produced in supernova remnants. *Astrophys. J.* **2013**, *763*, 47. [CrossRef]
2. Boos, E.; Lebedev, I.; Philippova, L. Modelling of an energy spectrum of cosmic rays in the knee region. *J. Phys. G Nucl. Part Phys.* **2006**, *32*, 2273–2278. [CrossRef]
3. Erlykin, A.D.; Wolfendale, A.W. Interpretation of features in the cosmic ray proton and helium energy spectra in terms of a local source. *J. Phys. G Nucl. Part. Phys.* **2015**, *42*, 125201. [CrossRef]
4. Kuzmichev, L.; Astapov, I.; Bezyazeekov, P.; Borodin, A.; Brückner, M.; Budnev, N.; Chiavassa, A.; Gress, O.; Gress, T.; Grishin, O.; et al. Cherenkov EAS arrays in the Tunka astrophysical center: From Tunka-133 to the TAIGA gamma and cosmic ray hybrid detector. *Nucl. Instrum. Methods Phys. Res. Sect. A Accel. Spectrometers Detect. Assoc. Equip.* **2020**, *952*, 161830. [CrossRef]
5. Apel, W.D.; Badea, A.; Bekk, K.; Blümer, J.; Boos, E.; Bozdog, H.; Brancus, I.; Daumiller, K.; Doll, P.; Engel, R. Applying shower development universality to KASCADE data. *Astropart. Phys.* **2008**, *29*, 412–419. [CrossRef]
6. Aguilar, M.; Cavasonza, L.A.; Alpat, B.; Ambrosi, G.; Arruda, L.; Attig, N.; Aupetit, S.; Azzarello, P.; Bachlechner, A.; Barao, F.; et al. Precision measurement of cosmic-ray nitrogen and its primary and secondary components with the alpha magnetic spectrometer on the International Space Station. *Phys. Rev. Lett.* **2018**, *121*, 051103. [CrossRef]
7. Mocchiutti, E. Direct detection of cosmic rays: Through a new era of precision measurements of particle fluxes. *Nucl. Phys. B* **2014**, *256–257*, 161–172. [CrossRef]
8. Adriani, O.; Barbarino, G.; Bazilevskaya, G.; Bellotti, R.; Boezio, M.; Bogomolov, E.; Bongi, M.; Bonvicini, V.; Bottai, S.; Bruno, A.; et al. The PAMELA Mission: Heralding a new era in precision cosmic ray physics. *Phys. Rep.* **2014**, *544*, 323. [CrossRef]
9. Borisov, S.V.; Voronov, S.A.; Karelin, A.V. Energy measurements of electrons and protons in cosmic ray physics using satellite and balloon calorimeters in recent two decades. *Cosm. Res.* **2011**, *49*, 247. [CrossRef]
10. Sparvoli, R. Direct measurements of cosmic rays in space. *Nucl. Phys. B Proc. Suppl.* **2013**, *239–240*, 115–122. [CrossRef]
11. Panov, A.D.; Adams, J.H.; Ahn, H.S.; Batkov, K.E.; Bashindzhagyan, G.L.; Watts, J.W.; Wefel, J.P.; Wu, J.; Ganel, O.; Guzik, T.G.; et al. Elemental energy spectra of cosmic rays from the data of the ATIC-2 experiment. *Bull. Russ. Acad. Sci. Phys.* **2007**, *71*, 494. [CrossRef]
12. Yoon, Y.S.; Ahn, H.S.; Allison, P.S.; Bagliesi, M.G.; Beatty, J.; Bigongiari, G.; Boyle, P.J.; Childers, J.T.; Conklin, N.B.; Coutu, S.; et al. Cosmic-ray proton and helium spectra from the first CREAM flight. *Astrophys. J.* **2011**, *728*, 122. [CrossRef]

13. Yoon, Y.S.; Anderson, T.; Barrau, A.; Conklin, N.B.; Coutu, S.; Derome, L.; Han, J.H.; Jeon, J.A.; Kim, K.C.; Kim, M.H.; et al. Proton and Helium Spectra from the CREAM-III Flight. *Astrophys. J.* **2017**, *839*, 5. [CrossRef]
14. Adriani, O.; Barbarino, G.C.; Bazilevskaya, G.A.; Bellotti, R.; Boezio, M.; Bogomolov, E.A.; Bongi, M.; Bonvicini, V.; Bottai, S.; Bruno, A.; et al. Ten years of PAMELA in space. *Riv. Nuovo Cim.* **2017**, *40*, 1.
15. Aguilar, M.; Aisa, D.; Alpat, B.; Alvino, A.; Ambrosi, G.; Andeen, K.; Arruda, L.; Attig, N.; Azzarello, P.; Bachlechner, A.; et al. Precision Measurement of the Proton Flux in Primary Cosmic Rays from Rigidity 1 GV to 1.8 TV with the Alpha Magnetic Spectrometer on the International Space Station. *Phys. Rev. Lett.* **2015**, *114*, 171103.
16. Atkin, E.; Bulatov, V.; Dorokhov, V.; Gorbunov, N.; Filippov, S.; Grebenyuk, V.; Karmanov, D.; Kovalev, I.; Kudryashov, I.; Kurganov, A.; et al. New Universal Cosmic-Ray Knee near a Magnetic Rigidity of 10 TV with the NUCLEON Space Observatory. *JETP Lett.* **2018**, *108*, 5. [CrossRef]
17. Adriani, O.; Akaike, Y.; Asano, K.; Asaoka, Y.; Bagliesi, M.G.; Berti, E.; Bigongiari, G.; Binns, W.R.; Bonechi, S.; Bongi, M.; et al. Direct Measurement of the Cosmic-Ray Proton Spectrum from 50 GeV to 10 TeV with the Calorimetric Electron Telescope on the International Space Station. *Phys. Rev. Lett.* **2019**, *122*, 181102. [CrossRef]
18. An, Q.; Asfandiyarov, R.; Azzarello, P.; Bernardini, P.; Bi, X.J.; Cai, M.S.; Chang, J.; Chen, D.Y.; Chen, H.F.; Chen, J.L.; et al. Measurement of the cosmic ray proton spectrum from 40 GeV to 100 TeV with the DAMPE satellite. *Sci. Adv.* **2019**, *5*, aax3793.
19. Haino, S.; Sanuki, T.; Abe, K.; Anraku, K.; Asaoka, Y.; Fuke, H.; Imori, M.; Itasaki, A.; Maeno, T.; Makida, Y.; et al. Measurements of primary and atmospheric cosmic-ray spectra with the BESS-TeV spectrometer. *Phys. Lett. B* **2004**, *594*, 35–46. [CrossRef]
20. Dmitriyeva, E.; Fedosimova, A.; Lebedev, I.; Temiraliev, A.; Abishev, M.; Kozhamkulov, T.; Mayorov, A.; Spitaleri, C. Determination of the primary energy using an ultrathin calorimeter. *J. Phys. G Nucl. Part. Phys.* **2020**, *47*, 035202. [CrossRef]
21. Allison, J.; Amako, K.; Apostolakis, J.; Arce, P.; Asai, M.; Aso, T.; Bagli, E.; Bagulya, A.; Banerjee, S.; Barrand, G.; et al. Recent developments in Geant4. *Nucl. Instrum. Methods Phys. Res. Sect. A Accel. Spectrometers Detect. Assoc. Equip.* **2016**, *835*, 186–225. [CrossRef]
22. Fedosimova, A.; Gaitinov, A.; Grushevskaya, E.; Lebedev, I. Study of the peculiarities of multiparticle production via event-by-event analysis in asymmetric nucleus-nucleus interactions. *EPJ Web. Conf.* **2017**, *145*, 19009. [CrossRef]
23. Fedosimova, A.; Gaitinov, A.S.; Lebedev, I.A.; Temiraliev, A. Study on initial geometry fluctuations via correlation of finite distributions of secondary particles in nucleus-nucleus interactions. *J. Phys. Conf. Ser.* **2016**, *668*, 012067. [CrossRef]
24. Kvochkina, T.N.; Lebedev, I.A.; Lebedeva, A.A. An analysis of high-energy interactions with large transverse momentum of secondary particles. *J. Phys. G Nucl. Part Phys.* **2000**, *26*, 35–41. [CrossRef]
25. Adamovich, M.I.; Andreeva, N.P.; Basova, E.S.; Bradnova, V.; Bubnov, V.I.; Chernyavsky, M.M.; Gaitinov, A.S.; Gulamov, K.G.; Haiduc, M.; Hasegan, D.; et al. Flow Effects in High-Energy Nucleus Collisions with Ag(Br) in Emulsion. *Phys. At. Nucl.* **2004**, *67*, 273–280. [CrossRef]
26. Adamovich, M.I.; Aggarwal, M.M.; Andreeva, N.P.; Badyal, S.K.; Bakich, A.M.; Basova, E.S.; Bhalla, K.B.; Bhasin, A.; Bhatia, V.S.; Bradnova, V.; et al. Factorial Moments of ^{28}Si Induced Interactions with Ag(Br) Nuclei. *APH N.S. Heavy Ion Phys.* **2001**, *13*, 213–221. [CrossRef]
27. Lipari, P. Universality in the longitudinal development of Cosmic Ray showers. *Nucl. Part. Phys. Proc.* **2016**, *279–281*, 111–117. [CrossRef]
28. Fedosimova, A.; Kharchevnikov, P.; Lebedev, I.; Temiraliev, A. Applying universality in the development of cascade processes for the research of high energy cosmic particles in space experiments. *EPJ Web. Conf.* **2017**, *145*, 10004. [CrossRef]
29. Tompakova, N.; Dmitriyeva, E.; Lebedev, I.; Serikkanov, A.; Grushevskaya, Y.; Mit', K.; Fedosimova, A. Influence of hydrogen plasma on SnO_2 thin films. *Mater. Today Proc.* **2020**, *25*, 83–87. [CrossRef]